FAST DIRECT: QUERY-EFFICIENT ONLINE BLACK-BOX GUIDANCE FOR DIFFUSION-MODEL TARGET GENERATION

Anonymous authors
Paper under double-blind review

ABSTRACT

Guided diffusion-model generation is a promising direction for customizing the generation process of a pre-trained diffusion-model to address the specific downstream tasks. Existing guided diffusion models either rely on training of the guidance model with pre-collected datasets or require the objective functions to be differentiable. However, for most real-world tasks, the offline datasets are often unavailable, and their objective functions are often not differentiable, such as image generation with human preferences, molecular generation for drug discovery, and material design. Thus, we need an **online** algorithm capable of collecting data during runtime and supporting a **black-box** objective function. Moreover, the **query efficiency** of the algorithm is also critical because the objective evaluation of the query is often expensive in the real-world scenarios. In this work, we propose a novel and simple algorithm, **Fast Direct**, for query-efficient online black-box target generation. Our Fast Direct builds a pseudo-target on the data manifold to update the noise sequence of the diffusion model with a universal direction, which is promising to perform query-efficient guided generation. Extensive experiments on twelve high-resolution (1024×1024) image target generation tasks and six 3D-molecule target generation tasks show **6**$\times$ up to **10**$\times$ query efficiency improvement and **11**$\times$ up to **44**$\times$ query efficiency improvement, respectively.

1 INTRODUCTION

Diffusion models have become the state-of-the-art generative model for image synthesis (Ho et al., 2020; Nichol & Dhariwal, 2021; Dhariwal & Nichol, 2021) and video synthesis (Ho et al., 2022), etc. Its remarkable success is due to its powerful capability in modeling the complex multi-mode high-dimensional data distributions.

One promising direction for utilizing the generative power of diffusion models is through target generation. This allows users to customize the generation process to meet specific downstream objectives, effectively extending the models' capabilities beyond synthesis problems to engineering optimization and science discovery problems, such as image generation with human preferences, drug discovery (Corso et al., 2022; Guan et al., 2023) and material design (Vlassis & Sun, 2023; Giannone et al., 2023).

The pre-trained diffusion models often struggle to generate desired samples for these applications, especially when the target data lies out of the training data distribution. Therefore, the target generation often involves model fine-tuning or guidance techniques. Krishnamoorthy et al. (2023) proposes to train the diffusion model with re-weighted training loss, while Clark et al. (2023); Black et al. (2023); Fan et al. (2024); Yang et al. (2024) advocates for fine-tuning the parameters of the pre-trained model. As oppose to training-time approaches, Bansal et al. (2023) introduces an inference-time approach, which replaces the classifier in classifier guidance (Dhariwal & Nichol, 2021) with a differentiable objective function to achieve the downstream target. However, the requirement of the differentiable objective limits the practical usage of it for real applications with black-box feedback.

Most real-world applications of target generation involve evaluating **black-box objectives** in an **online** manner. For example, image generation with human preferences requires human users to evaluate the generated images; drug design requires real-world experiments to evaluate the generated

molecules. These applications typically require several iterative query-feedback cycles with a black-box objective to achieve satisfactory target generation. As objective evaluations are often expensive, it becomes crucial to develop **query-efficient** algorithms to minimize the cost of these evaluations.

Although the **online black-box** target generation tasks are important, the existing works are not suitable to address this task. Bansal et al. (2023); Krishnamoorthy et al. (2023); Lu et al. (2023) require training an offline guidance model with pre-collected data, while Bansal et al. (2023); Clark et al. (2023); Prabhudesai et al. (2023); He et al. (2023) require the objective function to be differentiable. Most recently, Black et al. (2023); Fan et al. (2024); Yang et al. (2024) can be employed for online black-box target generation, but they require online updates of the huge number of the parameters, which is both time-consuming and not query-efficient.

In Section 3.1, we first propose a novel guided noise sequence optimization (GNSO) technique to guide the diffusion model sampling process towards a given target. GNSO updates the noise sequence in a *universal direction* on the data manifold. Our GNSO is **efficient**: it enables fast adaptation (with around only 50 steps) from any initial generation towards the given input target. Moreover, GNSO is **robust**: empirically, even the input target image is noisy, it can still generate a clear image semantically similar to the target image. The GNSO itself cannot directly handle black-box target generation tasks, but it provides a backbone for further designing black-box algorithms.

In Section 3.2, based on our GNSO technique, we further propose a novel algorithm, **Fast Direct**, to tackle the **online black-box** target generation tasks in a **query-efficient** manner. Fast Direct builds a pseudo-target on the data manifold as the input for our GNSO, to guides the diffusion model at inference time. Notably, our Fast Direct is easy to implement and support any stochastic diffusion scheduler. Moreover, our Fast Direct provides a very flexible framework for extension. Any designs of update methods for the pseudo-target can serve as a plug-in for our Fast Direct.

In Section 4, we evaluate our Fast Direct algorithm on the real-world applications: high-resolution (1024×1024) image target generation tasks and 3D-molecule target generation tasks. For image tasks, we employ the black-box API of the modern Large Language Model (LLM), Gemini 1.5, as the black-box objective, which is much more practical compared with the synthetic toy score function used in the literature. Extensive experiments on twelve image target generation tasks and six 3D-molecule target generation tasks show significant query efficiency improvement: **6**-times up to **10**-times query efficiency improvement on image tasks and **11**-times up to **44**-times query efficiency improvement on 3D-molecule tasks, compared with baselines. Additionally, we evaluate Fast Direct on compressibility, incompressibility, and atheistic quality tasks, demonstrating its generalization ability on the unseen prompts. Our contributions are summarized as follows:

- We propose a novel guided noise sequence optimization (GNSO) technique to guide the diffusion model sampling process toward a given target in an efficient and robust manner.
- Based on GNSO, we further propose a novel algorithm, Fast Direct, to address online black-box target generation tasks in a query-efficient manner.
- Fast Direct acheives significant query efficiency improvement in the real-world applications: high-resolution image target generation tasks and 3D-molecule target generation tasks. Additionally, we demonstrate its generalization capability for unseen prompts.

2 Related Works

2.1 Guided Generation

Diffusion guided generation (also called inference-time guidance) refers to the technique to guide the sampling trajectory of the pre-trained diffusion to generate target data (Croitoru et al., 2023; Chen et al., 2024). The key advantage of this approach is that it does not require updating the model parameters, which is computationally expensive, especially for large models.

Dhariwal & Nichol (2021) proposed classifier guidance. However, it requires a guidance model that trained on noisy images with different noise scales, which generally not readily available and often requires training from scratch for each domain. Chung et al. (2022); Bansal et al. (2023); He et al. (2023) extend the classifier guidance by using a differentiable objective function that is defined only for clean data. Instead of using noisy images, the predicted clean images at each sampling steps are used as the input for the guidance objective function. In this way, the guidance process can operate

on the clean image space. While the predicted clean image is naturally imperfect, empirically it still provide informative feedback to guide image generation (Bansal et al., 2023).

However, this approximation can harm image quality. Bansal et al. (2023) proposed universal guidance that comprises of backward guidance followed by a self-recurrence step to preserve image quality. On the other hand, He et al. (2023) leverages the differentiability of a well-trained auto-encoder to project the image to the data manifold and thus preserve image quality during the guidance process. Instead of guiding the sampling trajectory, Karunratanakul et al. (2024); Eyring et al. (2024) treat the diffusion process as a black-box and only optimize the initial (prior) noise.

While the aforementioned approaches assume a differentiable objective function, Lu et al. (2023) tackles black-box objective f by learning a differentiable proxy neural network h to match their gradients, i.e., $\nabla f \approx \nabla h$. Li et al. (2024) eliminates the need for a differentiable proxy model by employing importance sampling weighted by the objective values during the sampling process. Most recently, DNO (Tang et al., 2024) proposes optimize the diffusion noise sequence by using ZO-SGD (Nesterov & Spokoiny, 2017) to tackle black-box objective function. However, it runs at the instance level; namely, each run only produces one image.

2.2 Diffusion-model Fine-tuning

Diffusion-model fine-tuning refer to the technique that updating the pre-trained diffusion-model parameters to improve its performance on a specific use case. In this section, we review the fine-tuning methods that support online learning of the black-box objective function.

Black et al. (2023); Fan et al. (2024) formulate the diffusion fine-tuning problem as a reinforcement learning (RL) problem within Markov Decision Processes (MDPs), and proposes an iterative algorithm to fine-tune diffusion model by using Proximal Policy Optimization (PPO) (Schulman et al., 2017; Uehara et al., 2024) loss function. Fan et al. (2024) integrates the PPO with a KL regularization to prevent the fine-tuned model deviated too much from the pre-trained model.

On the other hand, Yang et al. (2024) does not requires an absolute objective values, instead it uses the relative reward on pair of samples by integrating DPO (Direct Preference Optimization) (Rafailov et al., 2024), a technique for fine-tuning large language models, into diffusion model.

Fine-tuning diffusion model requires large amount of GPU memory. Existing works mitigates the memory consumption by using LoRA (Low-Rank Adaptation) (Hu et al., 2021) technique, and only fine-tune parameters of the attention blocks in UNet. We categorize the related works based on whether they support the online and black-box objective tasks in Appendix F Table 2.

3 Methods

In this section, we first present a novel inference-time guidance generation method by guided noise sequence optimization. Based on this method, we further present our query-efficient online black-box guidance algorithm, Fast Direct, to address online black-box guidance tasks.

3.1 Noise Sequence Optimization with Target Guidance

Take i.i.d. Gaussian samples $\{\boldsymbol{\epsilon}_0, \cdots, \boldsymbol{\epsilon}_K\} \sim \mathcal{N}(\mathbf{0}, \boldsymbol{I})$, for $k \in \{1, \cdots, K\}$, the inference process of the diffusion model can be formulated as follows:

$$\boldsymbol{x}_k = \mathcal{S}_\theta(\boldsymbol{x}_{k-1}, \boldsymbol{\epsilon}_k), \tag{1}$$

where $\mathcal{S}_\theta(\cdot, \cdot)$ denotes the diffusion model sampler that depends on the concrete SDE solver used, $\boldsymbol{x}_0 = \boldsymbol{\epsilon}_0$ is a Gaussian sample, and $\boldsymbol{x}_K$ denotes the generated data.

Question 1: Given an input target $\boldsymbol{x}^*$, can we guide a pre-trained diffusion model at inference time to generate the target data in an efficient and robust manner?

To answer this question, we need to develop an algorithm to address two challenges simultaneously: (1) Guidance Efficiency: the algorithm can use only a few iteration steps of guidance update to generate target data $\boldsymbol{x}^*$. (2) Robust to noisy target: given a noisy target (e.g., a noise perturbed image), the algorithm can generate meaningful target data (e.g., a clear image).

Algorithm 1 Guided Noise Sequence Optimization

1: **Input:** stepsize α, target data $\boldsymbol{x}^*$, number of diffusion sampling step K, pre-trained diffusion sampler $\mathcal{S}_\theta$. Number of iteration T.
2: Take i.i.d. noise $\{\boldsymbol{\epsilon}_0, \cdots, \boldsymbol{\epsilon}_K\} \sim \mathcal{N}(\mathbf{0}, \boldsymbol{I})$.
3: Compute the norm of noise $\{\|\boldsymbol{\epsilon}_0\|, \cdots, \|\boldsymbol{\epsilon}_K\|\}$.
4: **for** $t = 1, \cdots, T$ **do**
5: /* Comment: Line 6- Line 9 call diffusion-model sampler to generate data $\boldsymbol{x}_K$ */
6: $\boldsymbol{x}_0 \leftarrow \boldsymbol{\epsilon}_0$
7: **for** $k = 1, \cdots, K$ **do**
8: $\boldsymbol{x}_k \leftarrow \mathcal{S}_\theta(\boldsymbol{x}_{k-1}, \boldsymbol{\epsilon}_k)$
9: **end for**
10: /* Comment: Line 11- Line 14 update the noise by moving along direction $\boldsymbol{x}^* - \boldsymbol{x}_K$ */
11: **for** $k = 0, \cdots, K$ **do**
12: $\hat{\boldsymbol{\epsilon}}_k \leftarrow \boldsymbol{\epsilon}_k + \alpha(\boldsymbol{x}^* - \boldsymbol{x}_K)$
13: $\boldsymbol{\epsilon}_k \leftarrow \frac{\hat{\boldsymbol{\epsilon}}_k}{\|\hat{\boldsymbol{\epsilon}}_k\|}\|\boldsymbol{\epsilon}_k\|$
14: **end for**
15: **end for**
16: Return target generation $\boldsymbol{x}_K$ and noise sequence $\{\boldsymbol{\epsilon}_0, \cdots, \boldsymbol{\epsilon}_K\}$

We propose a novel guided noise sequence optimization method to address the above two challenges, which is presented in Algorithm 1. Our method optimizes the noise sequence by updating noise along direction on data manifold. Specifically, Algorithm 1 consists of two procedures: data generation procedure and noise update procedure. In data generation procedure, Line 6- Line 9 in Algorithm 1 employ current noise sequence $\{\boldsymbol{\epsilon}_0, \cdots, \boldsymbol{\epsilon}_K\}$ to generate a data $\boldsymbol{x}_K$. In noise update procedure, Line 11- Line 14 in Algorithm 1, we update each noise $\boldsymbol{\epsilon}_k$ by moving along a universal direction $\boldsymbol{x}^* - \boldsymbol{x}_K$. Then, Algorithm 1 continues to employ the updated noise to generate a new data $\boldsymbol{x}_K$. By looping the data generation procedure and noise update procedure, Algorithm 1 can generate a clear and meaningful target.

The direction $\boldsymbol{x}^* - \boldsymbol{x}_K$ point from the current generation data $\boldsymbol{x}_K$ to the target $\boldsymbol{x}^*$. Intuitively, moving in this direction will shift the diffusion sampling trajectory toward the target. We highlight the advantage of updating noise with the *universal direction* $\boldsymbol{x}^* - \boldsymbol{x}_K$ compared with direction $\boldsymbol{x}^* - \boldsymbol{x}_k$ as the following remark.

Remark: In our Algorithm 1, we guided the noise update by moving along a universal direction $\boldsymbol{x}^* - \boldsymbol{x}_K$. This direction lies in the data manifold, which alleviates the quality degeneration of the generated data. We employ the direction $\boldsymbol{x}^* - \boldsymbol{x}_K$ instead of the direction $\boldsymbol{x}^* - \boldsymbol{x}_k$ because the internal $\boldsymbol{x}_k$ during inference sampling process may be far away from the data manifold (e.g., the $\boldsymbol{x}_k$ can be a very noisy and distorted image), which may degenerate the quality.

We empirically evaluate Algorithm 1 with different update directions: $\vec{d} = \boldsymbol{x}^* - \boldsymbol{x}_K$ and $\vec{d} = \boldsymbol{x}^* - \boldsymbol{x}_k$. Additionally, we consider the approximation $\boldsymbol{x}_K \approx \hat{\boldsymbol{x}}_k$[1]. Lastly, we set the noisy target to test the robustness. We use the stable-diffusion model as the pre-trained model. The stepsize α is set to $\alpha = 2 \times 10^{-3}$. We present the generated images at every 10-iteration for each cases in Figure 1.

From Figure 1, we can observe that Algorithm 1 (with update direction $\boldsymbol{x}^* - \boldsymbol{x}_K$) can successfully guide the diffusion process towards the target image, while $\boldsymbol{x}^* - \boldsymbol{x}_k$ leads to a degenerated image. The approximation $\boldsymbol{x}^* - \hat{\boldsymbol{x}}_K$ can achieve comparable target image but not as accurate as $\boldsymbol{x}^* - \boldsymbol{x}_K$.

Interestingly, even the input target $\boldsymbol{x}^*$ is perturbed by noise and lies out of the data manifold, Algorithm 1 will generate a pseudo-data on data manifold that is similar to the noisy target $\boldsymbol{x}^*$ but with much higher quality compared with the input noisy target. This property is important for designing black-box guidance methods because the update direction is an approximation or estimation of the true gradient of the black-box objective.

Moreover, we present the updating direction $\boldsymbol{x}^* - \boldsymbol{x}_{K'}$ for $K' \in \{K, K/2, K/4, K/8\}$ in Appendix C. We observe that the generated image quality decreases as the $\boldsymbol{x}_{K'}$ becomes more noisy.

[1]The $\hat{\boldsymbol{x}}_k$ is the "predicted clean image" at step k, see the Eq.12 of DDIM (Song et al., 2020). Note that it is undefined for initial step, so we simple set $\hat{\boldsymbol{x}}_0 \coloneqq \hat{\boldsymbol{x}}_1$.

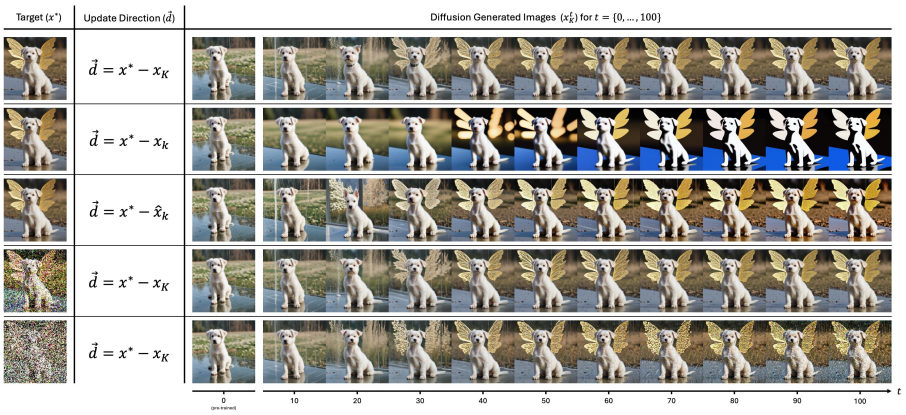

Figure 1: Demonstration of guided generation for a given target by Algorithm 1. Column 2 (Update Direction) indicates the update term of Algorithm 1 Line 12. Row 1 to 3 analyze how different update directions can affect the generated images. Row 4 and 5 show that by using the update direction of $\boldsymbol{x}^* - \boldsymbol{x}_K$, diffusion model is able to generate visually satisfied images even when the target image is noisy. The noisy target image ($\boldsymbol{x}^*$) of the row 4 is obtained by clean image added with noise $\mathcal{N}(\mathbf{0}, \boldsymbol{I})$, and row 5 is added with noise $\mathcal{N}(\mathbf{0}, 9 \times \boldsymbol{I})$.

3.2 QUERY-EFFICIENT ONLINE BLACK-BOX GUIDANCE

In section 3.1, we address the diffusion guidance sampling with a given optimal target input. However, in reality, we often only have access to the black-box objective function $f(\boldsymbol{x})$, where the optimal target data $\boldsymbol{x}^* = \arg\min f(\boldsymbol{x})$ is unknown. In this section, we further investigate the diffusion guidance sampling with only black-box objective feedback. For this task, it is natural to ask the following question.

Question 2: Can we guide a pre-trained diffusion model at inference time to generate target data with only black-box objective feedback in a query-efficient online manner?

To answer this question, we need to address two challenges: (1) Black-box challenge and (2) Online guidance challenge. The black-box challenge means that we cannot access the gradient of the objective. The online guidance challenge means we don't have a prior dataset to train a surrogate (classifier) for guidance; we can only access the black-box objective through query feedback online. Usually, the query evaluation is expensive. Thus, the query efficiency is critical.

Algorithm 2 Fast Direct

Input: Max number of batch queries N, batch size B, step-size α, number of diffusion sampling step K, pre-trained diffusion sampler $\mathcal{S}_\theta$
Initialization: $\mathcal{D} = \{\}$.
for $i = 1, \cdots, N$ **do**
  Take i.i.d. noise $\{\boldsymbol{\epsilon}_0, \cdots, \boldsymbol{\epsilon}_K\} \sim \mathcal{N}(\mathbf{0}, \boldsymbol{I})$.
  Compute the norm of noise $\{\|\boldsymbol{\epsilon}_0\|, \cdots, \|\boldsymbol{\epsilon}_K\|\}$.
  for $t = 1, \cdots, i$ **do**
    $\boldsymbol{x}_0 \leftarrow \boldsymbol{\epsilon}_0$
    for $k = 1, \cdots, K$ **do**
      $\boldsymbol{x}_k \leftarrow \mathcal{S}_\theta(\boldsymbol{x}_{k-1}, \boldsymbol{\epsilon}_k)$
    end for
    Set a pseudo target $\hat{\boldsymbol{x}}^*$ by a nonparametric method.
    for $k = 0, \cdots, K$ **do**
      $\hat{\boldsymbol{\epsilon}}_k \leftarrow \boldsymbol{\epsilon}_k + \alpha(\hat{\boldsymbol{x}}^* - \boldsymbol{x}_K)$
      $\boldsymbol{\epsilon}_k \leftarrow \frac{\hat{\boldsymbol{\epsilon}}_k}{\|\hat{\boldsymbol{\epsilon}}_k\|}\|\boldsymbol{\epsilon}_k\|$
    end for
  end for
  Query black-box objective score $y = f(\boldsymbol{x}_K)$
  Increment dataset $\mathcal{D} \leftarrow \mathcal{D} \cup \{(\boldsymbol{x}_K, y)\}$
end for

We start addressing the above two challenges based on our target guidance generation Algorithm 1. Although Algorithm 1 itself cannot handle black-box guidance tasks because it needs input a target $\boldsymbol{x}^*$, it provides a basis for us to design query efficient online black-box guidance methods. To be specific, Algorithm 1 enables us to generate a target even updating with a noisy direction $\boldsymbol{x}^* - \boldsymbol{x}_K$. This property is important for black-box guidance tasks because we can use a noisy estimation of the gradient of the black-box objective to guide the generation.

The key idea is to set a pseudo target $\hat{\boldsymbol{x}}^*$ to guide the generation process based on our Algorithm 1. We present our Fast Direct method as in Algorithm 2. In Algorithm 2, we call Algorithm 1 inside the for-loop w.r.t. the number of batch queries t. The only difference compared with Alg. 1 is that we set a pseudo target $\hat{\boldsymbol{x}}^*$ in Line 11 of Algorithm 2 instead of a given fixed target $\boldsymbol{x}^*$.

The choice of models for updating the pseudo target $\hat{\boldsymbol{x}}^*$ in Algorithm 2 is flexible, which supports various black-box target generation method designs based on our Fast Direct algorithm framework. In this work, we set the pseudo target $\hat{\boldsymbol{x}}^*$ through nonparametric methods without additional training. Specifically, we employ two methods for setting the pseudo target $\hat{\boldsymbol{x}}^*$, namely, Gaussian process (GP) update and historical optimal update.

Set pseudo target $\hat{\boldsymbol{x}}^*$ by GP update: For the GP update case, we set the pseudo target $\hat{\boldsymbol{x}}^*$ as the one gradient step update using the gradient of the posterior mean prediction of the GP surrogate model as follows:

$$\hat{\boldsymbol{x}}^* = \boldsymbol{x}_K - \nabla \hat{f}(\boldsymbol{x}_K; \boldsymbol{X}^n) \tag{2}$$

where $\boldsymbol{x}_K$ denotes the generated data in Algorithm 2 and $\hat{f}(\boldsymbol{x}_K; \boldsymbol{X}^n)$ denotes the posterior prediction of the GP surrogate model (Seeger, 2004) evaluated at $\boldsymbol{x}_K$, which has closed-form as below:

$$\hat{f}(\boldsymbol{x}_K; \boldsymbol{X}^n) = \boldsymbol{k}(\boldsymbol{x}_K, \boldsymbol{X}^n)^\top \big(\mathcal{K}(\boldsymbol{X}^n, \boldsymbol{X}^n) + \lambda \boldsymbol{I}\big)^{-1} \boldsymbol{y} \tag{3}$$

where $\boldsymbol{X}^n = [\boldsymbol{x}^1, \cdots, \boldsymbol{x}^n]$ and $\boldsymbol{y} = [y^1, \cdots, y^n]$ denotes the collected data and its corresponding score value in the historical set $\mathcal{D}$ in Algorithm 2, respectively. When the historical set $\mathcal{D}$ is empty, we simply set the gradient $\nabla \hat{f}(\boldsymbol{x}_K; \varnothing) = 0$.

In this work, we employ shift-invariant kernels that can be rewritten in the form as $k(\boldsymbol{z}_1, \boldsymbol{z}_2) = g(\|\boldsymbol{z}_1 - \boldsymbol{z}_2\|_2)$, e.g., Gaussian kernel and Matérn kernel. We show that the gradient of the GP surrogate when employing these shift-invariant kernels lies on the low-dimensional data manifold. We present this property in Proposition 1. Detailed proof of Proposition 1 can be found in Appendix E. This property enables us to generate meaningful data on the data manifold instead of degenerated data, which is important for high-dimensional diffusion-model target generation problems, e.g., high-resolution (1024×1024) target image generation tasks.

Proposition 1. *Given prior data $\boldsymbol{X}^n = [\boldsymbol{x}^1, \cdots, \boldsymbol{x}^n]$ and its corresponding score $\boldsymbol{y} = [y^1, \cdots, y^n]$, let $\hat{f}(\boldsymbol{x}; \boldsymbol{X}^n)$ denotes the posterior mean of the GP model. For shift-invariant kernels $k(\boldsymbol{z}_1, \boldsymbol{z}_2) = g(\|\boldsymbol{z}_1 - \boldsymbol{z}_2\|_2)$, $\nabla \hat{f}(\boldsymbol{x}; \boldsymbol{X}^n)$ lies on a subspace spanned by $[\boldsymbol{x}, \boldsymbol{x}^1, \cdots, \boldsymbol{x}^n]$, where $\boldsymbol{x}^i$ denotes the i^{th} data sample in $\boldsymbol{X}^n$.*

Remark: When setting the pseudo target $\hat{\boldsymbol{x}}^*$ as Eq.(2), we know the pseudo target $\hat{\boldsymbol{x}}^*$ lies on the low-dimensional subspace spanned by data according to Proposition 1. Usually, the gradient descent update in Eq.(2) will lead to a new pseudo target $\hat{\boldsymbol{x}}^*$ with a lower score. In addition, based on the empirical observation from Algorithm 1, we know even the pseudo target $\hat{\boldsymbol{x}}^*$ is noisy, Algorithm 1 can still generate similar data that is meaningful lies on the data manifold. These two properties enable Algorithm 2 to generate data with lower and lower scores along the data manifold.

Set pseudo target $\hat{\boldsymbol{x}}^*$ by historical optimal update: For the historical optimal update case, we set pseudo target $\hat{\boldsymbol{x}}^*$ as the empirical optimal point from the historical dataset $\mathcal{D}$ in Algorithm 2 as:

$$\hat{\boldsymbol{x}}^* = \arg\min_{\boldsymbol{x} \in \mathcal{D}} f(\boldsymbol{x}). \tag{4}$$

Set pseudo target $\hat{\boldsymbol{x}}^*$ as Eq.(4) is an empirical approximation of the optimal target $\boldsymbol{x}^* = \arg\min_{\boldsymbol{x} \in \mathcal{X}} f(\boldsymbol{x})$. In Algorithm 2, at each iteration w.r.t. the batch query i, we employ the generated data that achieves the current best score as the pseudo target $\hat{\boldsymbol{x}}^*$ to guide the generation process. Intuitively, given this pseudo target $\hat{\boldsymbol{x}}^*$, Algorithm 2 will generate a batch of data that is similar to $\hat{\boldsymbol{x}}^*$ on the low-dimensional data manifold, which is promising to further improve the score. By looping this procedure, we will get data generation with lower and lower scores.

4 EXPERIMENTS

In this section, we evaluate our algorithm in two domains, images and molecules, and compare it against four baseline methods: DDPO (Black et al., 2023), DPOK (Fan et al., 2024), D3PO (Yang et al., 2024), DNO (Tang et al., 2024). Moreover, we further evaluate our algorithm in compressibility, incompressibility, and aesthetic quality tasks in Appendix A. Our source code will be made public available upon publication.

4.1 IMAGE BLACK-BOX TARGET GENERATION TASK

Problem: Prompt Alignment. We consider the image-prompt alignment problem. While the current state-of-the-art image generative models excel at generating highly realistic images, they sometime struggle to faithfully generate images that accurately aligned with the input prompts, especially those complex prompts involving rare object combinations, object counting, or specific object positioning.

Pre-trained Model: SDXL-Lightning. We use SDXL (Podell et al., 2023) diffusion model as the backbone text-to-image model. It is able to generate 1024×1024 high resolution realistic image. In our experiment, we use the distilled version, SDXL-Lightning (Lin et al., 2024), for its high sampling efficiency, which can generate image with comparable quality with just $K = 8$ steps. We use the official implementation [2]

Objective Function: Gemini 1.5. We leverage Gemini 1.5 (Reid et al., 2024), an advanced multimodal LLM service, as our black-box objective function to evaluate the alignment between input prompts and generated images. To avoid confusion, the term *query* refers to the input to Gemini, while *prompt* refers to the text used for image generation.

The query to Gemini 1.5 composes of the generated images with the question like: "Does the prompt `$prompt` accurately describe the image? Rate from 1 to 5". We state the complete query in Appendix G.

Because it is a closed-source paid service, we limit the number of batch queries in our experiments, referred to as the *batch queries budget*. We use the Gemini 1.5 Flash model (code: `gemini-1.5-flash-001`) for its cost-efficiency, and set the temperature as 0 for experiments consistency and reproducibility. For conciseness, we call it simply *Gemini* in the following section.

Experiment Procedure. We identify 12 prompts that the pre-trained model SDXL-Lighning struggles to generate, and refer these as the 12 tasks in our experiment, where the goal is to generate images that accurately aligned with the input prompts. We compare our Fast Direct algorithm against each baselines methods, and each experiment is constrained with 50 of batch queries budget.

We perform inference-time guidance using Fast Direct (Algorithm 2) to maximize the Gemini rating. We use the GP model in Eq. 2 for the pseudo-target, and set the kernel as Gaussian kernel, and we follow (Hvarfner et al., 2024) to set the lengthscale as $\lambda = \sqrt{d}$, where $d = 4\times128\times128$ is the latents dimensionality of SDXL. We use $N = 50$ iterations to utilize 50 batch queries budget, and set the batch size as $B = 32$ and step size as $\alpha = 80$. We use the `EularDescreteScheduler` (Karras et al., 2022) sampler as suggested by the SDXL-Lightning implementation (Lin et al., 2024), and the `DDIMScheduler` (Song et al., 2020) (DDIM) sampler for a fair comparison with the baselines.

For all baseline methods, we perform 50 iterations, each iteration utilizes one batch query for updating. We set the batch size as 32, and leave the rest of the hyper-parameters as default. We state more details for baselines in the Appendix. Note that for DNO, in which each experiment trial can only produce one image, we run 16 independent experiment trials and report the average results[3].

Experiment Results. We present the results for the "deer-elephant" [4] task in this section and defer the results for the other 11 tasks to Appendix I due to space constraints. We compare the images generated by our method with those generated by the baseline methods at each 10 batch queries intervals in Fig. 2. We can observe that our algorithm successfully satisfies the visual objectives

[2] https://huggingface.co/ByteDance/SDXL-Lightning

[3] Note that DNO spent $16 \times 50 = 800$ batch queries for each task.

[4] The complete prompt is: `A yellow reindeer and a blue elephant.`

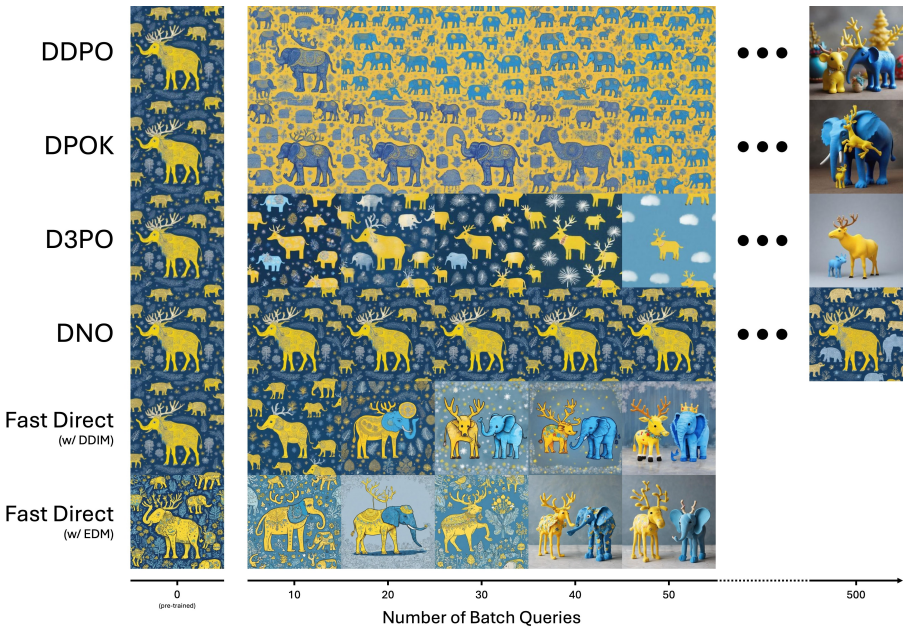

Figure 2: The generated images over each number of batch queries on the prompt "deer-eleplant" [4], extra batch queries budgets (until 500) are given to the baselines methods for demonstration.

for both samplers within the 50 batch queries budget, while the baseline methods fall short within the same budget. Similar phenomenon are observed for the other 11 tasks in Appendix I. We grant baseline methods with extra batch queries budget, and we observed that DDPO and DPOK almost achieves the visual objectives, whereas D3PO and DNO remain unsuccessful in this particular task.

We collect the 32 randomly generated images using our algorithm (by utilizing 50 batch queries budget) and present in Fig. 3. We can observe that most images are well satisfies the visual objective. Similar phenomenon are observed on the other 11 tasks as shown in Appendix I.

For the quantitative results, we report the average objective values over each batch query across the 12 tasks in Fig. 4. For DNO, which only produces one image each experiment, we average the results from 16 independent experiments. We observe that the Fast Direct achieves nearly full score within the 50 batch queries budget in all tasks, which is significant higher than the baseline methods. Moreover, we observe that Fast Direct achieve similar score for both samplers, suggesting it is invariant to sampler. We further perform ablation study in Appendix B, and show that Fast Direct is insensitive to the hyper-parameters: step size α and batch size B.

We further employ tasks 1 to 3 and assigns extra batch queries budget of 200 to the baseline methods. We report the *accumulated objective values*, which represents the best objective values achieved up to each number of batch queries, in Appendix Fig. 11. We observe that our algorithm, utilizing only 50 batch queries budget, consistently outperforms all baseline methods even when they are assigned with expanded batch queries budget of 200.

To quantify this advantage, in Table 1, we identify the minimum number of batch queries budget (denotes as N^*) our algorithm requires to surpass each baseline methods with their 200 batch query budget. We further calculate ours *batch-query-efficiency gain* compared to baselines as $\frac{200}{N^*}$ and report (in the bracket) in Table 1. We can observe that our algorithm is at least 667% and up to 1000% more batch-queries-efficient than the baseline methods.

4.2 Molecule Black-box Target Generation Task

Problem: Drug Discovery. We consider the drug discovery problem. One of the key problem is to find drug molecules that has a strong binding affinity with the target protein receptor. The binding affinity quantify the strength of the interaction between two bio-molecules, so a stronger binding affinity indicates a higher drug efficacy.

A traditional approach to this problem requires human-design molecules, which are highly time-consuming. Recent advancements in AI poses a great potential to speedup this process by generating molecules using advanced generative model such as diffusion model. Although the cur-

Figure 3: The 32 randomly generated image for the prompt "deer-eleplant" [4] guided by Fast Direct (w/ EDM) by utilizing 50 batch queries budget.

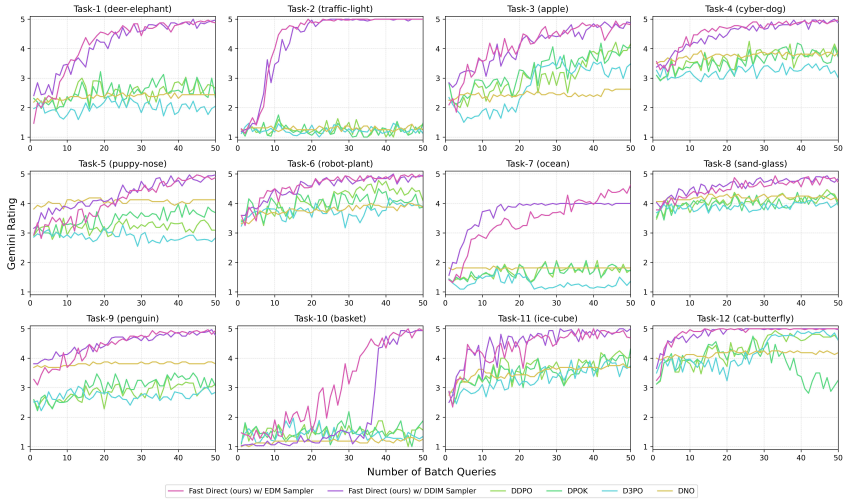

Figure 4: The average Gemini rating (from 1 to 5, higher is better) of the generated images over each number of batch queries on the 12 different tasks (the prompts abbreviation shown in bracket, see the complete prompts in Appendix 3).

rent pre-trained molecules models, such as TargetDiff, are capable of generating relatively realistic molecules, it lacks the ability of generating molecules with user desired high binding affinity.

Pre-trained Model: TargetDiff. We use TargetDiff (Guan et al., 2023) as the backbone molecules generative model. It is pre-trained on the CrossDocked2020 dataset (Francoeur et al., 2020), and can generate realistic 3D molecular structures conditioned on the given protein receptor. For sampling efficiency, we use the `DDIMScheduler` sampler with $K = 200$ sampling steps as we find that it can generate comparable results. During the generation process, we fix the atoms type according to the dataset reference and only allow the atoms position to be varied. We use the official implementation [5] in our experiment.

Objective Function: Molecules Binding Affinity. Measurement of the binding affinity requires real-world experiment which is highly expensive (David et al., 2020). In our experiment, we leverage the Vina score (kcal/mol) calculated by the AutoDock Vina simulation software (Eberhardt et al., 2021) to estimate the binding affinity. A lower (more negative) Vina score indicates a stronger estimated binding affinity. Therefore, our objective is to minimize the Vina score.

Experiment Procedure. We conduct experiments on 6 tasks, where the goal of each task is to optimize the Vina score on the protein receptors of ID from 1 to 6, respectively. Similar to images tasks, each algorithm is constrained with 50 of batch queries budget.

[5] https://github.com/guanjq/targetdiff

Table 1: The minimum number of batch queries budget (denotes as N^*) for Fast Direct (ours) to outperform each baselines (when each baseline is granted with 200 batch queries budget) on images and molecules tasks. The values in bracket show the batch-query-efficiency gain ($\frac{200}{N^*}$) of Fast Direct (ours) over the baselines.

	Minimum number of batch queries (N^*) for **Fast Direct** to outperform each baselines:		
	DDPO	**DPOK**	**D3PO**
Image Tasks			
Task 1	15 (13.34×)	15 (13.34×)	10 (20.00×)
Task 2	8 (25.00×)	8 (25.00×)	4 (50.00×)
Task 3	37 (5.41×)	46 (4.34×)	16 (12.50×)
Average	20 (10.00×)	23 (8.70 ×)	30 (6.67×)
Molecules Tasks			
Task 1	6 (33.33×)	5 (40.00×)	25 (8.00×)
Task 2	9 (22.22×)	4 (50.00×)	11 (18.18×)
Average	7.5 (26.67×)	4.5 (44.44×)	18 (11.11×)

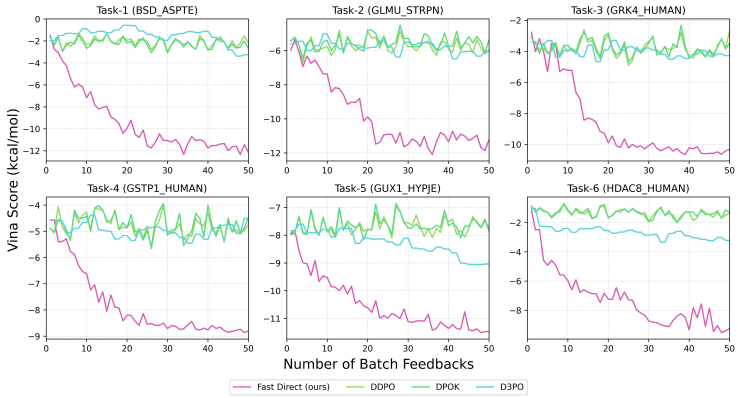

Figure 5: The Vina score (lower is better) of the generated molecules for each number batch queries on the six protein receptors.

We perform inference-time guidance using our Algorithm 2 to minimize the Vina score. We use the historical optimal in Eq. 4 for the pseudo-target. We use $N = 50$ iterations to utilize 50 batch queries budget, and set the batch size as $B = 32$, and the step size as $\alpha = 10^{-2}$. We then conduct experiments on the baseline methods for 50 fine-tuning iteration. For DDPO and DPOK, the batch size is set as the same 32; while D3PO requires binary rewards, so we double the batch size as 64 [6]. We keep the hyper-parameters as default for all baseline methods.

Experiment Results. We report the average Vina score (recall, lower is better) for each batch queries across 6 tasks in Fig. 5. We observe that our algorithm consistently achieves much lower Vina score compared to the baseline methods across all tasks. Similar to the images task, we grant extra batch queries budget of 200 to the baselines for task 1 and 2, and report the *accumulated objective values* in Appendix Fig 12, and list the *batch-query-efficiency gain* in Table 1. We observe that our algorithm is at least 1111% and up to 4444% more batch-query-efficient compared to the baseline methods.

5 Conclusion

In this work, we proposed **Fast Direct** for diffusion model target generation, which effectively addresses the challenges of limited batch query budgets and black-box objective functions, demonstrating its potential for various applications, including image generation and drug discovery. Fast Direct is highly practical, as it is easy to implement, supports any type of SDE solver, and has only one hyper-parameter to tune (step size α). Our algorithm is based on the surprising empirical observation that the *universal update direction* (i.e., $\boldsymbol{x}^* - \boldsymbol{x}_K$ in Algorithm 1) can efficiently guide the diffusion trajectory toward the target, even when the target $\boldsymbol{x}^*$ is extremely noisy. This phenomenon suggests an intriguing robustness in the diffusion inference process. Future research could investigation for its underlying theoretical principles.

[6] However, unlike image tasks where Gemini can evaluate rewards for two images in a single query, the Vina simulation lacks this capability, requiring 64 individual queries for a batch of size 64.

REFERENCES

Arpit Bansal, Hong-Min Chu, Avi Schwarzschild, Soumyadip Sengupta, Micah Goldblum, Jonas Geiping, and Tom Goldstein. Universal guidance for diffusion models. In *Proceedings of the IEEE/CVF Conference on Computer Vision and Pattern Recognition*, pp. 843–852, 2023.

Kevin Black, Michael Janner, Yilun Du, Ilya Kostrikov, and Sergey Levine. Training diffusion models with reinforcement learning. *arXiv preprint arXiv:2305.13301*, 2023.

Minshuo Chen, Song Mei, Jianqing Fan, and Mengdi Wang. An overview of diffusion models: Applications, guided generation, statistical rates and optimization. *arXiv preprint arXiv:2404.07771*, 2024.

Hyungjin Chung, Jeongsol Kim, Michael T Mccann, Marc L Klasky, and Jong Chul Ye. Diffusion posterior sampling for general noisy inverse problems. *arXiv preprint arXiv:2209.14687*, 2022.

Kevin Clark, Paul Vicol, Kevin Swersky, and David J Fleet. Directly fine-tuning diffusion models on differentiable rewards. *arXiv preprint arXiv:2309.17400*, 2023.

Gabriele Corso, Hannes Stärk, Bowen Jing, Regina Barzilay, and Tommi Jaakkola. Diffdock: Diffusion steps, twists, and turns for molecular docking. *arXiv preprint arXiv:2210.01776*, 2022.

Florinel-Alin Croitoru, Vlad Hondru, Radu Tudor Ionescu, and Mubarak Shah. Diffusion models in vision: A survey. *IEEE Transactions on Pattern Analysis and Machine Intelligence*, 45(9): 10850–10869, 2023. doi: 10.1109/TPAMI.2023.3261988.

Laurianne David, Amol Thakkar, Rocío Mercado, and Ola Engkvist. Molecular representations in ai-driven drug discovery: a review and practical guide. *Journal of Cheminformatics*, 12(1):56, 2020.

Prafulla Dhariwal and Alexander Nichol. Diffusion models beat gans on image synthesis. *Advances in neural information processing systems*, 34:8780–8794, 2021.

Jerome Eberhardt, Diogo Santos-Martins, Andreas F Tillack, and Stefano Forli. Autodock vina 1.2. 0: New docking methods, expanded force field, and python bindings. *Journal of chemical information and modeling*, 61(8):3891–3898, 2021.

Luca Eyring, Shyamgopal Karthik, Karsten Roth, Alexey Dosovitskiy, and Zeynep Akata. Reno: Enhancing one-step text-to-image models through reward-based noise optimization. *arXiv preprint arXiv:2406.04312*, 2024.

Ying Fan, Olivia Watkins, Yuqing Du, Hao Liu, Moonkyung Ryu, Craig Boutilier, Pieter Abbeel, Mohammad Ghavamzadeh, Kangwook Lee, and Kimin Lee. Reinforcement learning for fine-tuning text-to-image diffusion models. *Advances in Neural Information Processing Systems*, 36, 2024.

Paul G Francoeur, Tomohide Masuda, Jocelyn Sunseri, Andrew Jia, Richard B Iovanisci, Ian Snyder, and David R Koes. Three-dimensional convolutional neural networks and a cross-docked data set for structure-based drug design. *Journal of chemical information and modeling*, 60(9):4200–4215, 2020.

Giorgio Giannone, Akash Srivastava, Ole Winther, and Faez Ahmed. Aligning optimization trajectories with diffusion models for constrained design generation. *Advances in Neural Information Processing Systems*, 36:51830–51861, 2023.

Jiaqi Guan, Wesley Wei Qian, Xingang Peng, Yufeng Su, Jian Peng, and Jianzhu Ma. 3d equivariant diffusion for target-aware molecule generation and affinity prediction. *arXiv preprint arXiv:2303.03543*, 2023.

Yutong He, Naoki Murata, Chieh-Hsin Lai, Yuhta Takida, Toshimitsu Uesaka, Dongjun Kim, Wei-Hsiang Liao, Yuki Mitsufuji, J Zico Kolter, Ruslan Salakhutdinov, et al. Manifold preserving guided diffusion. *arXiv preprint arXiv:2311.16424*, 2023.

Jonathan Ho, Ajay Jain, and Pieter Abbeel. Denoising diffusion probabilistic models. *Advances in neural information processing systems*, 33:6840–6851, 2020.

Jonathan Ho, Tim Salimans, Alexey Gritsenko, William Chan, Mohammad Norouzi, and David J Fleet. Video diffusion models. *Advances in Neural Information Processing Systems*, 35:8633–8646, 2022.

Edward J Hu, Yelong Shen, Phillip Wallis, Zeyuan Allen-Zhu, Yuanzhi Li, Shean Wang, Lu Wang, and Weizhu Chen. Lora: Low-rank adaptation of large language models. *arXiv preprint arXiv:2106.09685*, 2021.

Carl Hvarfner, Erik Orm Hellsten, and Luigi Nardi. Vanilla bayesian optimization performs great in high dimension. *arXiv preprint arXiv:2402.02229*, 2024.

Tero Karras, Miika Aittala, Timo Aila, and Samuli Laine. Elucidating the design space of diffusion-based generative models. *Advances in neural information processing systems*, 35:26565–26577, 2022.

Korrawe Karunratanakul, Konpat Preechakul, Emre Aksan, Thabo Beeler, Supasorn Suwajanakorn, and Siyu Tang. Optimizing diffusion noise can serve as universal motion priors. In *Proceedings of the IEEE/CVF Conference on Computer Vision and Pattern Recognition*, pp. 1334–1345, 2024.

Siddarth Krishnamoorthy, Satvik Mehul Mashkaria, and Aditya Grover. Diffusion models for black-box optimization. *arXiv preprint arXiv:2306.07180*, 2023.

Xiner Li, Yulai Zhao, Chenyu Wang, Gabriele Scalia, Gokcen Eraslan, Surag Nair, Tommaso Biancalani, Aviv Regev, Sergey Levine, and Masatoshi Uehara. Derivative-free guidance in continuous and discrete diffusion models with soft value-based decoding. *arXiv preprint arXiv:2408.08252*, 2024.

Shanchuan Lin, Anran Wang, and Xiao Yang. Sdxl-lightning: Progressive adversarial diffusion distillation. *arXiv preprint arXiv:2402.13929*, 2024.

Cheng Lu, Huayu Chen, Jianfei Chen, Hang Su, Chongxuan Li, and Jun Zhu. Contrastive energy prediction for exact energy-guided diffusion sampling in offline reinforcement learning. In *International Conference on Machine Learning*, pp. 22825–22855. PMLR, 2023.

Yurii Nesterov and Vladimir Spokoiny. Random gradient-free minimization of convex functions. *Foundations of Computational Mathematics*, 17(2):527–566, 2017.

Alexander Quinn Nichol and Prafulla Dhariwal. Improved denoising diffusion probabilistic models. In *International conference on machine learning*, pp. 8162–8171. PMLR, 2021.

Dustin Podell, Zion English, Kyle Lacey, Andreas Blattmann, Tim Dockhorn, Jonas Müller, Joe Penna, and Robin Rombach. Sdxl: Improving latent diffusion models for high-resolution image synthesis. *arXiv preprint arXiv:2307.01952*, 2023.

Mihir Prabhudesai, Anirudh Goyal, Deepak Pathak, and Katerina Fragkiadaki. Aligning text-to-image diffusion models with reward backpropagation. *arXiv preprint arXiv:2310.03739*, 2023.

Rafael Rafailov, Archit Sharma, Eric Mitchell, Christopher D Manning, Stefano Ermon, and Chelsea Finn. Direct preference optimization: Your language model is secretly a reward model. *Advances in Neural Information Processing Systems*, 36, 2024.

Machel Reid, Nikolay Savinov, Denis Teplyashin, Dmitry Lepikhin, Timothy Lillicrap, Jean-baptiste Alayrac, Radu Soricut, Angeliki Lazaridou, Orhan Firat, Julian Schrittwieser, et al. Gemini 1.5: Unlocking multimodal understanding across millions of tokens of context. *arXiv preprint arXiv:2403.05530*, 2024.

Christoph Schuhmann. Laion aesthetics. `https://laion.ai/blog/laion-aesthetics/`, August 2022.

John Schulman, Xi Chen, and Pieter Abbeel. Equivalence between policy gradients and soft q-learning. *arXiv preprint arXiv:1704.06440*, 2017.

Matthias Seeger. Gaussian processes for machine learning. *International journal of neural systems*, 14(02):69–106, 2004.

Jiaming Song, Chenlin Meng, and Stefano Ermon. Denoising diffusion implicit models. *arXiv preprint arXiv:2010.02502*, 2020.

Jiaming Song, Qinsheng Zhang, Hongxu Yin, Morteza Mardani, Ming-Yu Liu, Jan Kautz, Yongxin Chen, and Arash Vahdat. Loss-guided diffusion models for plug-and-play controllable generation. In *International Conference on Machine Learning*, pp. 32483–32498. PMLR, 2023.

Zhiwei Tang, Jiangweizhi Peng, Jiasheng Tang, Mingyi Hong, Fan Wang, and Tsung-Hui Chang. Tuning-free alignment of diffusion models with direct noise optimization. *arXiv preprint arXiv:2405.18881*, 2024.

Masatoshi Uehara, Yulai Zhao, Tommaso Biancalani, and Sergey Levine. Understanding reinforcement learning-based fine-tuning of diffusion models: A tutorial and review. *arXiv preprint arXiv:2407.13734*, 2024.

Nikolaos N Vlassis and WaiChing Sun. Denoising diffusion algorithm for inverse design of microstructures with fine-tuned nonlinear material properties. *Computer Methods in Applied Mechanics and Engineering*, 413:116126, 2023.

Bram Wallace, Meihua Dang, Rafael Rafailov, Linqi Zhou, Aaron Lou, Senthil Purushwalkam, Stefano Ermon, Caiming Xiong, Shafiq Joty, and Nikhil Naik. Diffusion model alignment using direct preference optimization. In *Proceedings of the IEEE/CVF Conference on Computer Vision and Pattern Recognition*, pp. 8228–8238, 2024.

Kai Yang, Jian Tao, Jiafei Lyu, Chunjiang Ge, Jiaxin Chen, Weihan Shen, Xiaolong Zhu, and Xiu Li. Using human feedback to fine-tune diffusion models without any reward model. In *Proceedings of the IEEE/CVF Conference on Computer Vision and Pattern Recognition*, pp. 8941–8951, 2024.

Hui Yuan, Kaixuan Huang, Chengzhuo Ni, Minshuo Chen, and Mengdi Wang. Reward-directed conditional diffusion: Provable distribution estimation and reward improvement. *Advances in Neural Information Processing Systems*, 36, 2024.

A MORE EXPERIMENTS: COMPRESSIBILITY, INCOMPRESSIBILITY, AND AESTHETIC QUALITY

Problem. We follow DDPO (Black et al., 2023) to evaluate our algorithm on the three black-box optimization tasks for images: compressibility, incompressibility, and aesthetic quality.

Objective Function. For compressibility, we aimed to minimize the compressed JPEG size (MB) of the generated images. For incompressibility, it's simply the inverse. For aesthetic quality, the aesthetic score is evaluated by the pre-trained LAION aesthetics predictor (Schuhmann, 2022), which is trained on human rating of the images aesthetic quality, and we aimed to maximize the aesthetic score.

Experiment Procedure. For each task, we uniformly sample from the 45 common animals (as proposed by DDPO (Black et al., 2023)) as input prompts and optimize the objective using Fast Direct in Algorithm 2. We set $N = 50$ batch queries budget for compressibility and incompressibility, and $N = 100$ for aesthetic quality. We use the same pre-trained model, hyper-parameters, and GP settings as in Section 4.1. The 45 common animals prompts used in the experiment is as follows:

cat	dog	horse	monkey	rabbit	zebra	spider	bird	sheep
deer	cow	goat	lion	tiger	bear	raccoon	fox	wolf
lizard	beetle	ant	butterfly	fish	shark	whale	dolphin	squirrel
mouse	rat	snake	turtle	frog	chicken	duck	goose	bee
pig	turkey	fly	llama	camel	bat	gorilla	hedgehog	kangaroo

Experiment Result. We present the objective scores for each task in the left column of Fig. 6 and provide the generated images for the three tasks in the supplementary materials. For compressibility and incompressibility, we observe that Fast Direct achieves significantly better scores than the baselines. For aesthetic quality, Fast Direct with the EDM sampler achieves significantly better scores than with DDIM, likely due to EDM being a more advanced sampler, capable of generating higher-quality images. DNO achieves comparable scores; however, note that each experiment optimizes and generates only a single image.

Generalization Ability. We follow DDPO to evaluate generalization ability. For Fast Direct, we freeze the learned GP model to generate 16 unseen images using distinct unseen animal prompts. Specifically, in this phase, Lines 17 and 18 are removed from Algorithm 2, and our algorithm does not access the objective function. For DDPO, DPOK, and D3PO, the fine-tuned models are frozen to generate images with the 16 unseen animal prompts. DNO is not applicable to this experiment because DNO needs to perform optimization for each image without generalization. For the unseen prompts, since DDPO didn't publish the unseen prompts, we created our own as follows:

elephant	eagle	pigeon	hippo	hamster	otter	panda	reindeer
owl	penguin	flamingo	seal	koala	giraffe	parrot	cheetah

In Fig.7, we present the images generated using the unseen prompt "hippo" by each algorithm across the three tasks. The remaining 15 prompts for the three tasks are provided in the supplementary material. A similar phenomenon is observed for all 15 other unseen prompts across the three tasks. For quantitative evaluation, we report the objective values for the unseen prompts in the right column of Fig.6. We can observe that Fast Direct with GP model has generalization ability to unseen prompts.

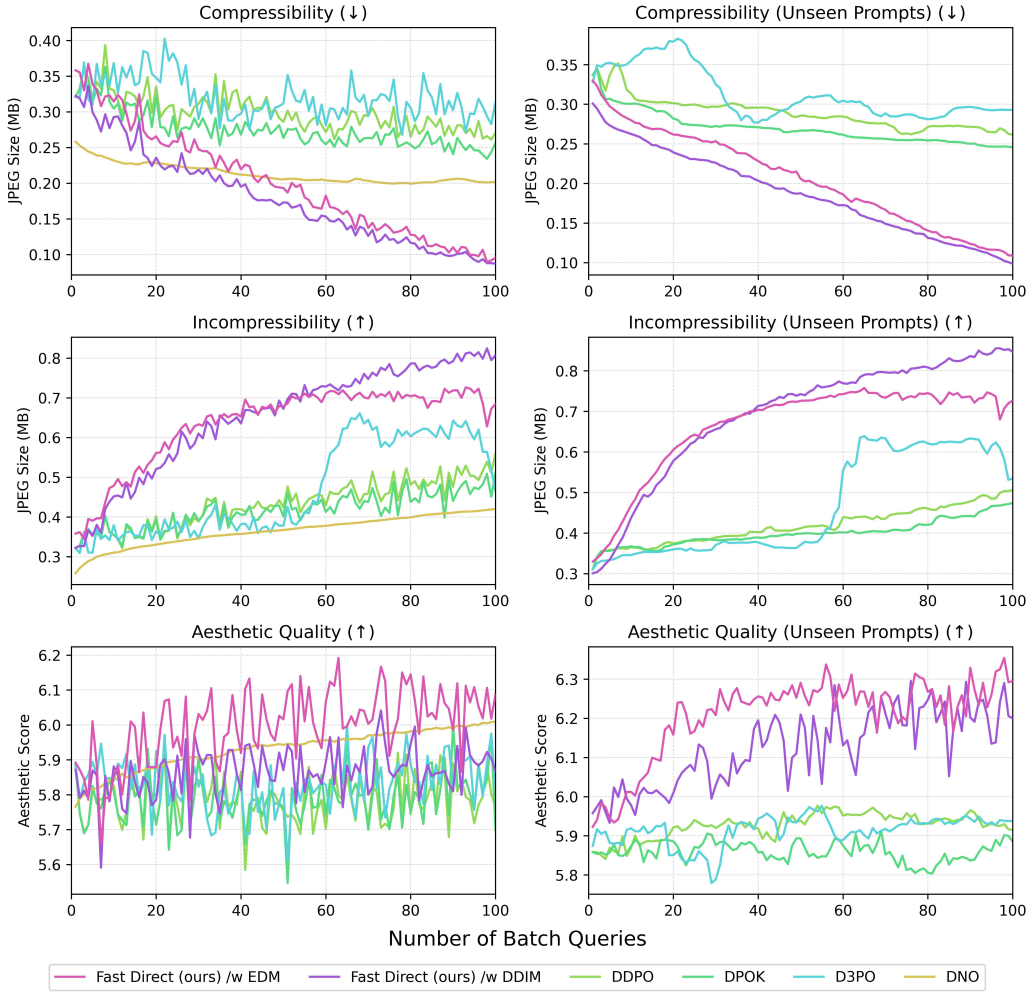

Figure 6: Left column: The average objective score of the generated images over each number of batch queries on the 3 black-box optimization tasks, the images are generated using the 45 common animals that used in DDPO (Tang et al., 2024) as the input prompts. Right column: The objective score of the images generated by **unseen prompts**, it demonstrates the generalization capability. Note that DNO is not applicable to this task.

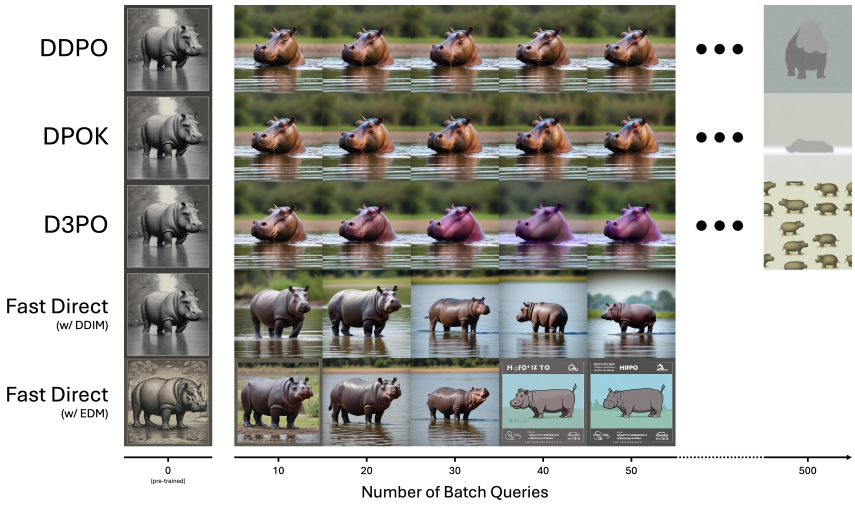

(a) Compressibility

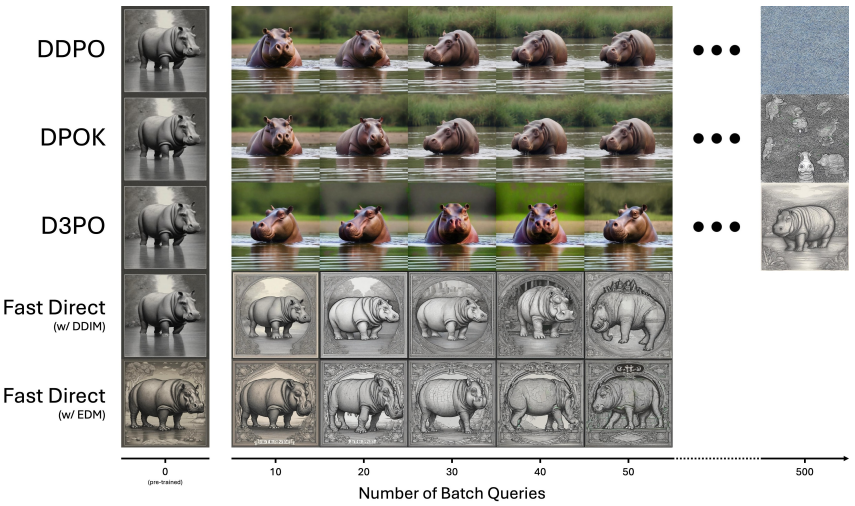

(b) Incompressibility

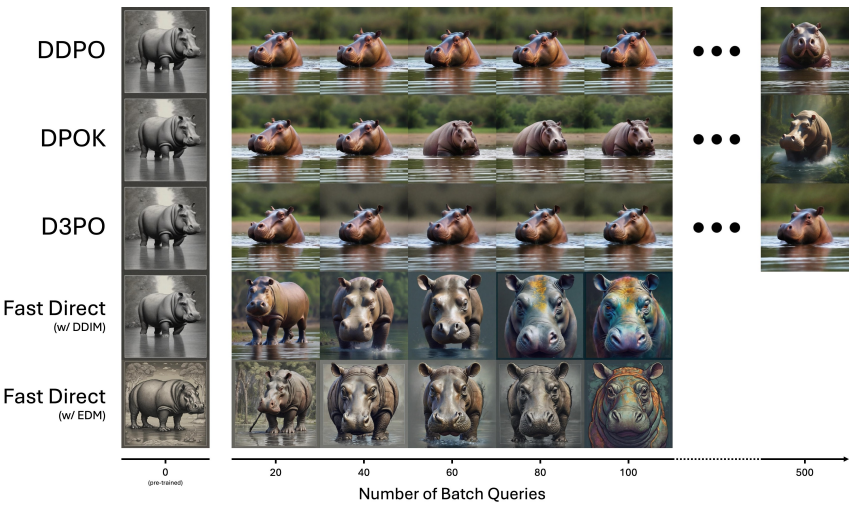

(c) Aesthetic Quality

Figure 7: The generated images using the unseen prompt "hippo" in aesthetic quality task, extra batch queries budgets (until 500) are given to the baselines methods for demonstration.

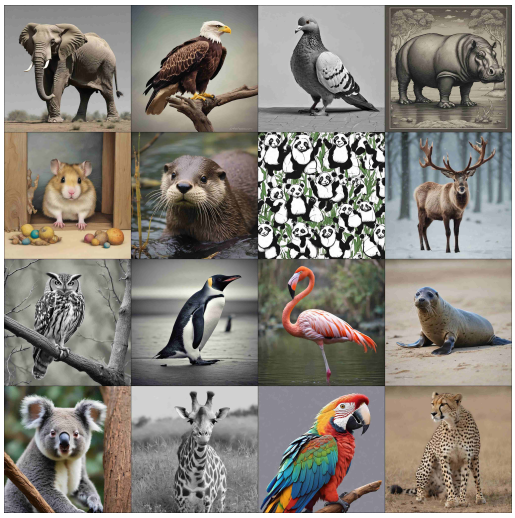

(a) Pre-trained

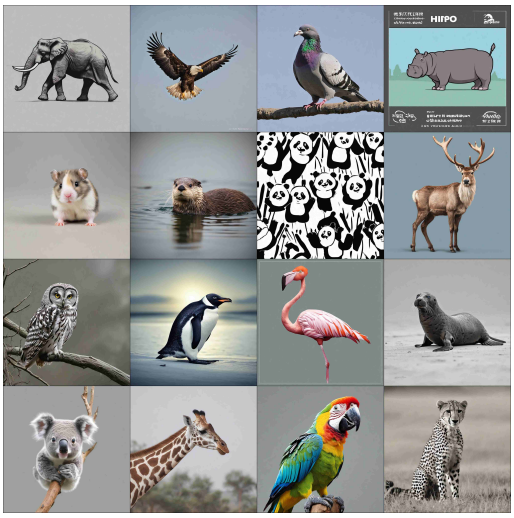

(b) Compressibility

(c) Incompressibility

(d) Aesthetic Quality

Figure 8: The generated images using the 16 unseen prompts. Top left is the images generated by pre-trained model, the rest are the Fast Direct generated images in the corresponding tasks.

B Ablation Study

We perform an ablation study on the target image generation Task-1. For step size analysis, we fix the batch size as 32, then perform experiment with different step size $\alpha = \{20, 40, 80, 160, 320\}$; for batch size analysis, we fix the step size as 80, then perform experiment with different batch size $B = \{4, 8, 16, 32, 64\}$. Additionally, we report the run time for different batch size. We report the result in Fig. 9.

We can observe that the performance steadily increase for any step size and any batch size, suggests that our algorithm is not sensitive to the hyper-parameters settings. The run time scales linearly with the batch size. In our target image generation experiments in Section 4.1, as the batch size is set as 32, each experiment takes approximately 6.4 hours to process 32 images in parallel.

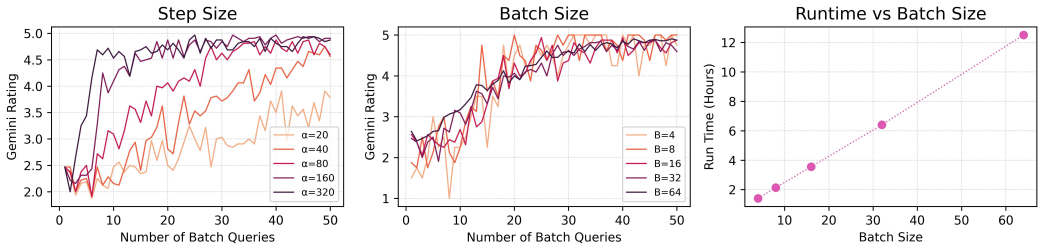

Figure 9: Left: Gemini rating for different step size settings. Middle: Gemini rating for different batch size settings. Right: Run time (hours) for different batch size settings.

C Analysis of Universal Direction

In Fig. 10, we demonstrate Algorithm 1 with update direction $\vec{d} = \boldsymbol{x}^* - \boldsymbol{x}_{K'}$ for $K' \in \{K, K/2, K/4, K/8\}$. It shows that the generated image quality decreases as the K' decreases. This is because as K' decreases, the $\boldsymbol{x}_{K'}$ becomes noisier and may move further away from the data manifold.

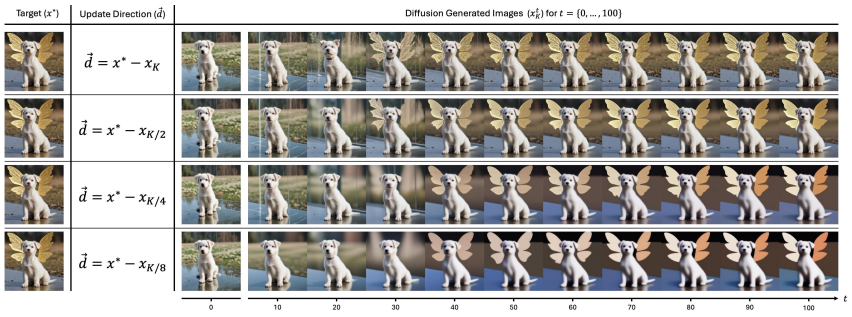

Figure 10: The update direction $\vec{d} = \boldsymbol{x}^* - \boldsymbol{x}_{K'}$ for $K' \in \{K, K/2, K/4, K/8\}$, the generated images quality decrease as the $\boldsymbol{x}_{K'}$ being more more noisy.

D Baselines Details

For DDPO, DPOK and D3PO, we fine-tune the model to maximize the Gemini rating. We fine-tune the model with 50 epochs; each epoch utilizes one batch query for model updating. For DDPO and DPOK, we set the batch size to 32; for D3PO, it requires a relative reward, so we doubled the batch size to 64.[7] As these RL-based methods require closed-form expression of the logarithm probabilities, we follow their official implementation to use the `DDIMScheduler` (Song et al., 2020) sampler.

[7]For D3PO, to evaluate 64 images only requires 32 queries calls, see Appendix G.

For DNO, we optimize the noise sequence w.r.t the Gemini rating. Recall that the Gemini is black-box, so we use the non-differentiable mode, with the number of samples for gradient approximation set as 32, and optimize for 50 iterations; each iteration utilizes one batch query for updating. However, each experiment of DNO only produces one image, where the score is highly dependent on the initial prior. Thus, for a more accurate evaluation, we run 16 independent experiments to generate 16 images and report the average results. Note that this requires $16 \times 50 = 800$ batch queries for each task, which is 16 times compared with our Fast Direct and other baselines.

E Proof of Proposition 1

Proof. Let $\boldsymbol{\alpha} = \left(\mathcal{K}(\boldsymbol{X}^n, \boldsymbol{X}^n) + \lambda \boldsymbol{I}\right)^{-1} \boldsymbol{y} = [\alpha_1, \cdots, \alpha_n]^\top$, for GP with a shift-invariant kernel that can be rewritten as $k(\boldsymbol{z}_1, \boldsymbol{z}_2) = g(\|\boldsymbol{z}_1 - \boldsymbol{z}_2\|_2)$, the gradient of the GP prediction is

$$\nabla \hat{f}(\boldsymbol{x}; \boldsymbol{X}^n) = \nabla \boldsymbol{k}(\boldsymbol{x}, \boldsymbol{X}^n)^\top \boldsymbol{\alpha} \tag{5}$$

$$= \sum_{i=1}^{n} \alpha_i \nabla k(\boldsymbol{x}, \boldsymbol{x}^i) \tag{6}$$

$$= \sum_{i=1}^{n} \frac{\alpha_i}{\|\boldsymbol{x} - \boldsymbol{x}^i\|} g'(\|\boldsymbol{x} - \boldsymbol{x}^i\|_2)(\boldsymbol{x} - \boldsymbol{x}^i) \tag{7}$$

$$= \sum_{i=1}^{n} c_i(\boldsymbol{x})(\boldsymbol{x} - \boldsymbol{x}^i) \tag{8}$$

where $\boldsymbol{x}^i$ denotes the i^{th} sample in $\boldsymbol{X}^n = [\boldsymbol{x}^1, \cdots, \boldsymbol{x}^n]$, and $c_i(\boldsymbol{x}) = \frac{\alpha_i}{\|\boldsymbol{x} - \boldsymbol{x}^i\|} g'(\|\boldsymbol{x} - \boldsymbol{x}^i\|_2)$, and $g'(\cdot)$ denotes the derivative of $g(\cdot)$.

From Eq.(8), we can see that the gradient $\nabla \hat{f}(\boldsymbol{x}; \boldsymbol{X}^n)$ is a weighted sum of $\boldsymbol{x} - \boldsymbol{x}^i$ for $i \in \{1, \cdots, n\}$. Thus, we know $\nabla \hat{f}(\boldsymbol{x}; \boldsymbol{X}^n)$ lies on a subspace spanned by $[\boldsymbol{x}, \boldsymbol{x}^1, \cdots, \boldsymbol{x}^n]$

□

F Overview of Related Works

We present the summary of related works according to its category and supported problem scenarios in Table 2.

Table 2: Overview of existing approaches.

Algorithm Category	Algorithm	Online	Black-box
Training / Fine-tune	DRaFT (Clark et al., 2023)	✓	✗
	DDOM (Krishnamoorthy et al., 2023), RCGDM (Yuan et al., 2024), DPO (Wallace et al., 2024)	✗	✓
	DDPO (Black et al., 2023), DPOK (Fan et al., 2024), D3PO (Yang et al., 2024)	✓	✓
Inference-time Guidance	LGD (Song et al., 2023), MPGD (He et al., 2023), DNO (2024a) (Karunratanakul et al., 2024), ReNO (Eyring et al., 2024)	✓	✗
	CEP (Lu et al., 2023)	✗	✓
	DNO (Tang et al., 2024), **Fast Direct** (ours)	✓	✓

G Experiment Details

We use the following query question to the Gemini:

```
Does the prompt $prompt accurately describe the image?
Rate from 1 (inaccurate) to 5 (accurate).
Answer in the format:  Score=(score), Reason=(reason).
```

where the `$prompt` is substituted by the input prompt used for image generation. We extract the integer score as the objective value.

The D3PO takes relative reward, so we specially crafted for its selective query question:

```
Given this two images, which image is better aligned with
the prompt $prompt?
Answer in the format:  Choice=(1/2), Reason=(reason).
```

where we extract the choice (1/2) as the selections.

The Gemini 1.5 Flash can faithfully respond with the correct format to ensure our experiment is consistent.

H More Experiment Results

We report the accumulated objective values over number of batch queries for images task in Fig. 11, and for molecules task in Fig. 12.

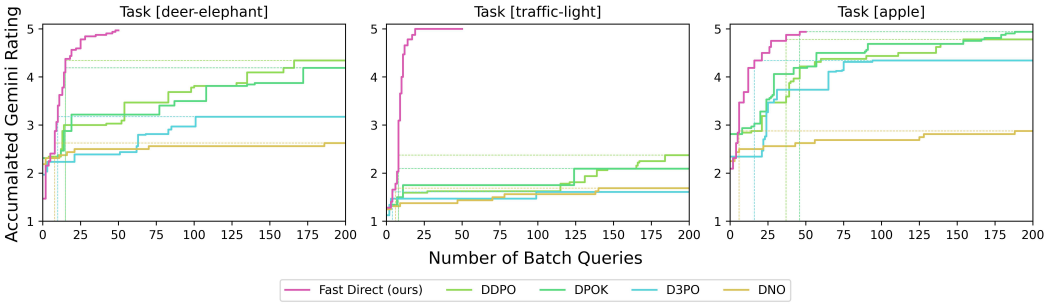

Figure 11: The accumulated Gemini rating (from 1 to 5, higher is better) over number of batch queries. The accumulated plot displays the maximum Gemini rating achieved up to each number of batch queries.

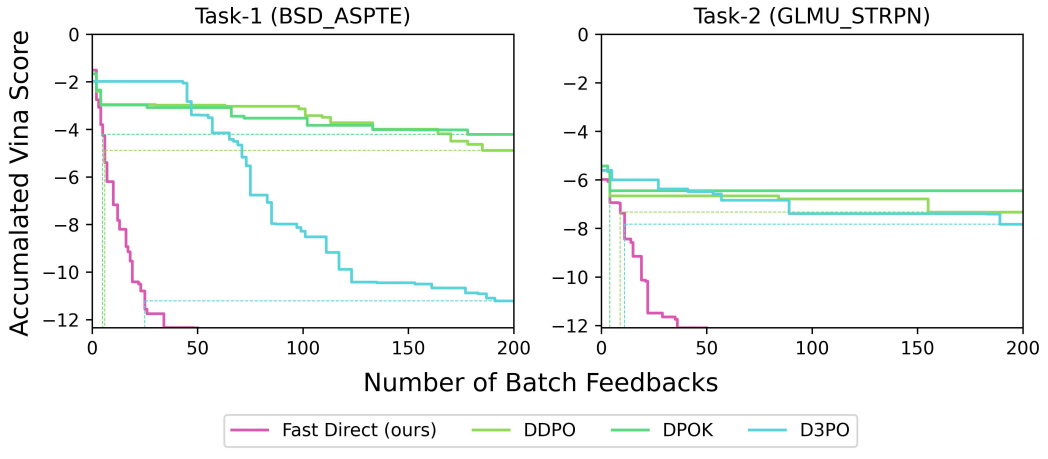

Figure 12: The accumulated Vina score (lower is better) over number of batch queries. The accumulated plot displays the minimum Vina score achieved up to each number of batch queries.

I MORE GENERATED IMAGES BY FAST DIRECT FOR IMAGE-PROMPT ALIGNMENT TASK

Table 3 shows the list the complete prompts used for each task in our image generation experiment. From Fig. 13 to Fig. 23, we present the generated images of each algorithms over each number of batch queries for prompt 2 to 12. From Fig. 24 to Fig. 34, we showcase the 32 randomly generated by pre-trained model followed by the resultant images guided by the Fast Direct for prompt 2 to 12.

Table 3: Target Image Generation Tasks

Task ID	Abbreviated Prompt	Complete Prompt
1	deer-elephant	A yellow reindeer and a blue elephant.
2	traffic-light	A traffic light with yellow at top, green at middle, and red at bottom.
3	apple	Seven red apples arranged in a circle.
4	cyber-dog	A natural fluffy dog talking to a cybertic dog.
5	puppy-nose	Side view of a puppy lying on floor, one butterfly stopping on its nose.
6	robot-plant	A cute cybernetic robot plants a tree in the forest.
7	ocean	A helicopter floating under the ocean.
8	sand-glass	A transparent glass filled with a mixture of water and sand, with one feather floating inside.
9	penguin	A photo realistic photo showing a penguin standing on a very small floating ice, with a tree is on fire in the background.
10	basket	Exactly one orange in a basket of apples.
11	ice-cube	A glass of water with exactly one ice cube.
12	cat-butterfly	A cat with butterfly wings.

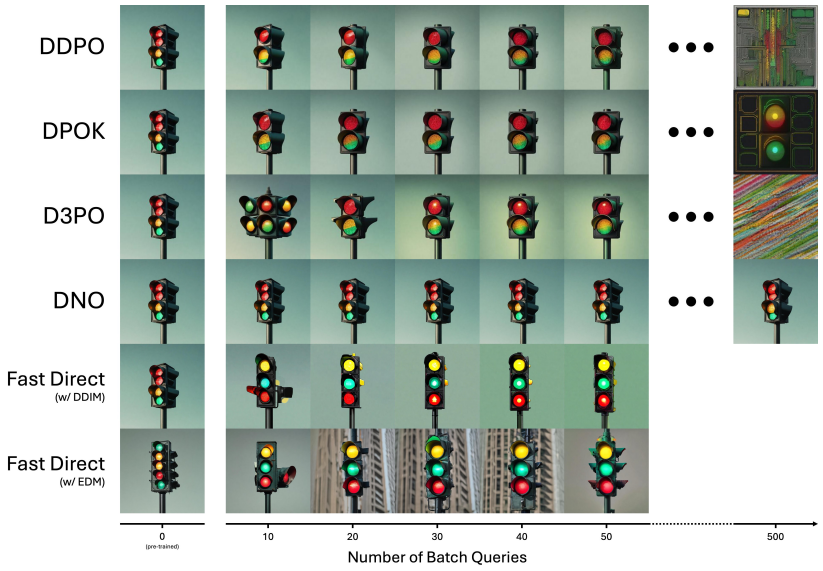

Figure 13: The generated images over each number of batch queries on the prompt ”traffic-light”, extra batch queries budgets (until 500) are given to the baselines methods for demonstration.

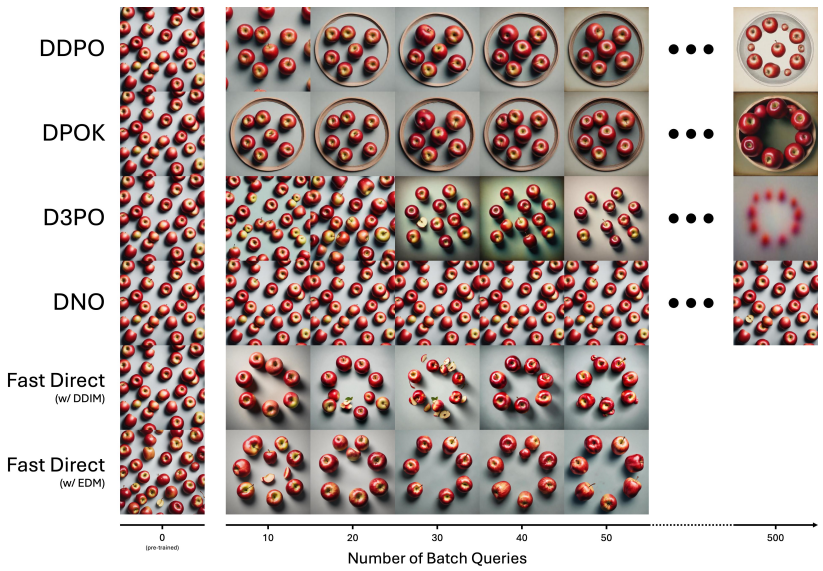

Figure 14: The generated images over each number of batch queries on the prompt ”apple”, extra batch queries budgets (until 500) are given to the baselines methods for demonstration.

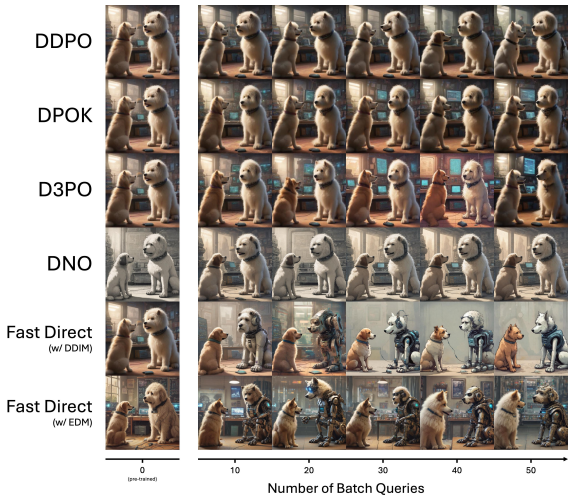

Figure 15: The generated images over each number of batch queries on the prompt ”cyber-dog” for each algorithms.

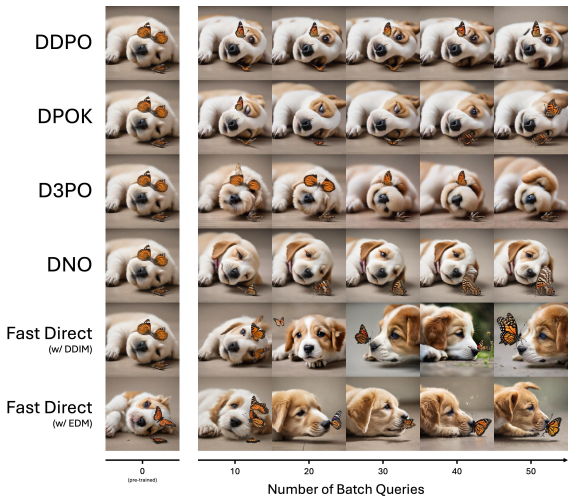

Figure 16: The generated images over each number of batch queries on the prompt ”puppy-nose” for each algorithms.

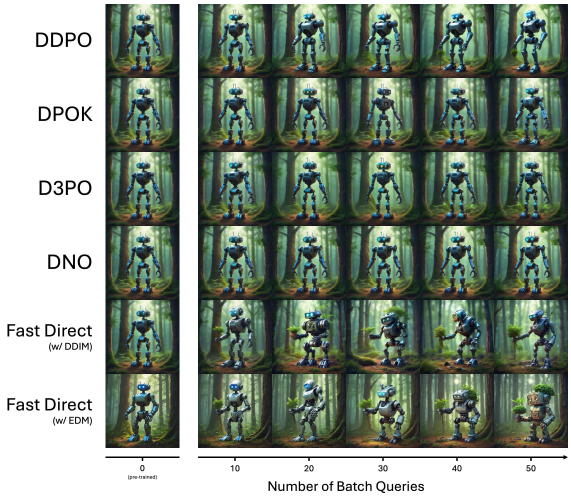

Figure 17: The generated images over each number of batch queries on the prompt ”robot-plant” for each algorithms.

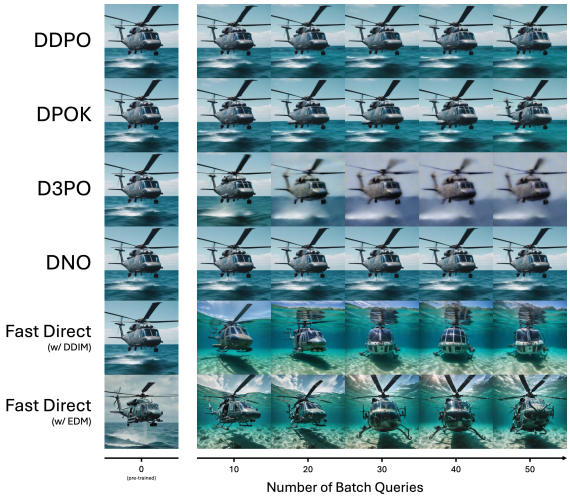

Figure 18: The generated images over each number of batch queries on the prompt ”ocean” for each algorithms.

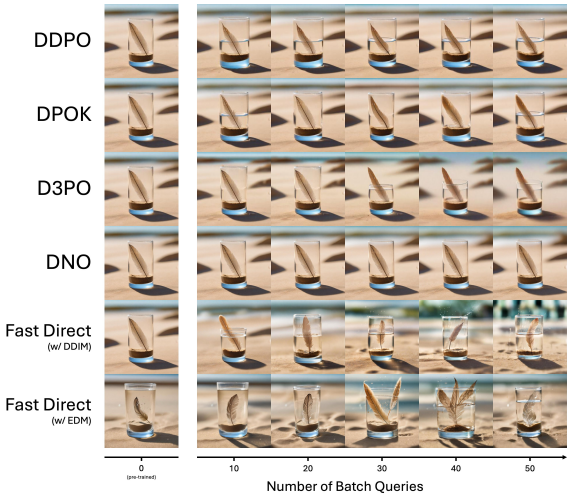

Figure 19: The generated images over each number of batch queries on the prompt ”sand-glass” for each algorithms.

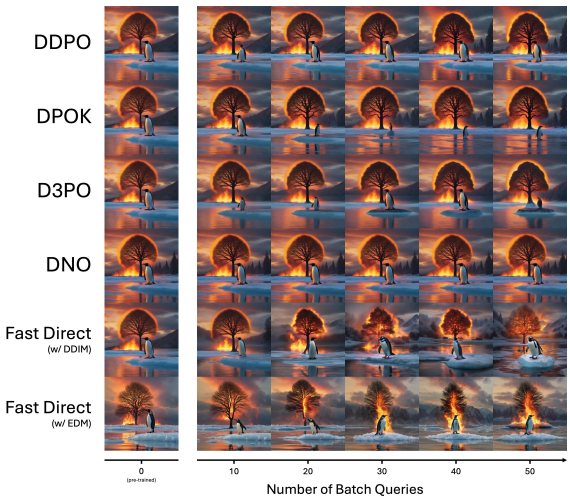

Figure 20: The generated images over each number of batch queries on the prompt ”penguin” for each algorithms.

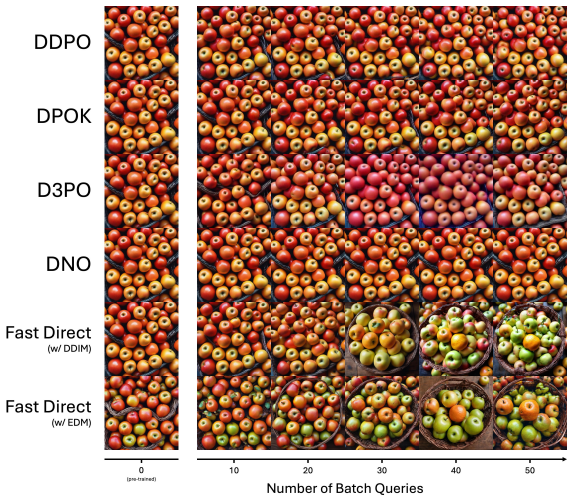

Figure 21: The generated images over each number of batch queries on the prompt ”basket” for each algorithms.

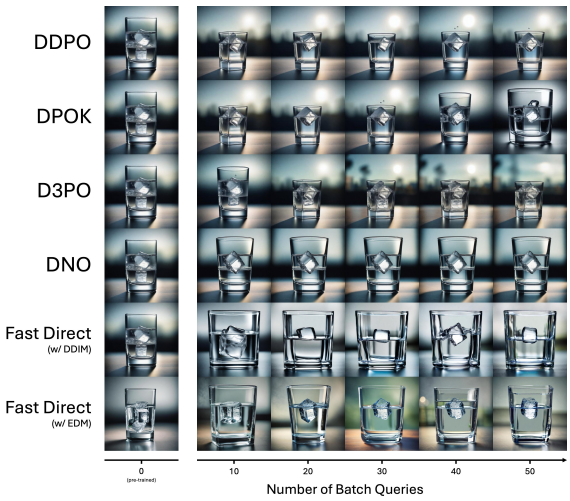

Figure 22: The generated images over each number of batch queries on the prompt ”ice-cube” for each algorithms.

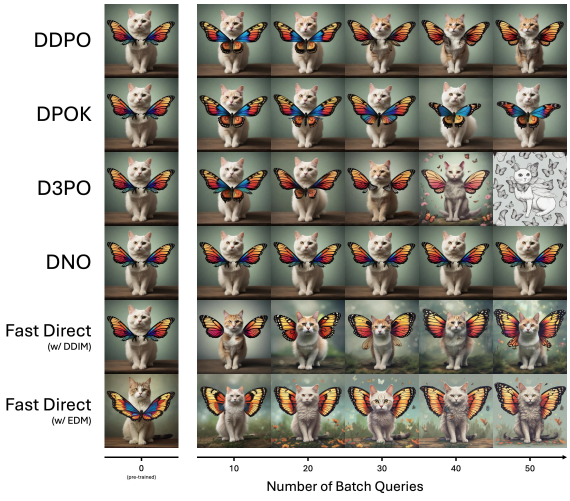

Figure 23: The generated images over each number of batch queries on the prompt ”cat-butterfly” for each algorithms.

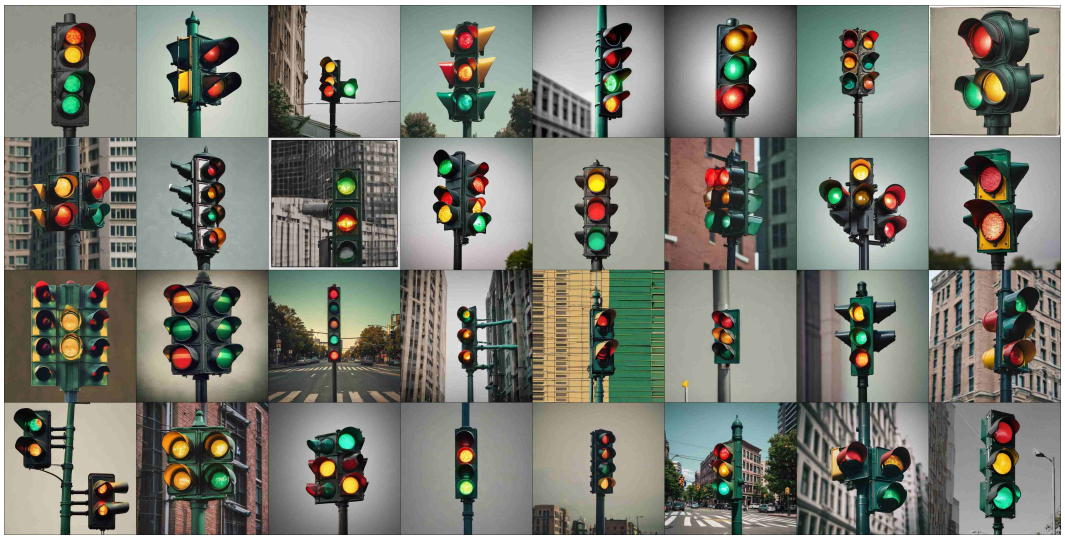

(a) Pre-trained

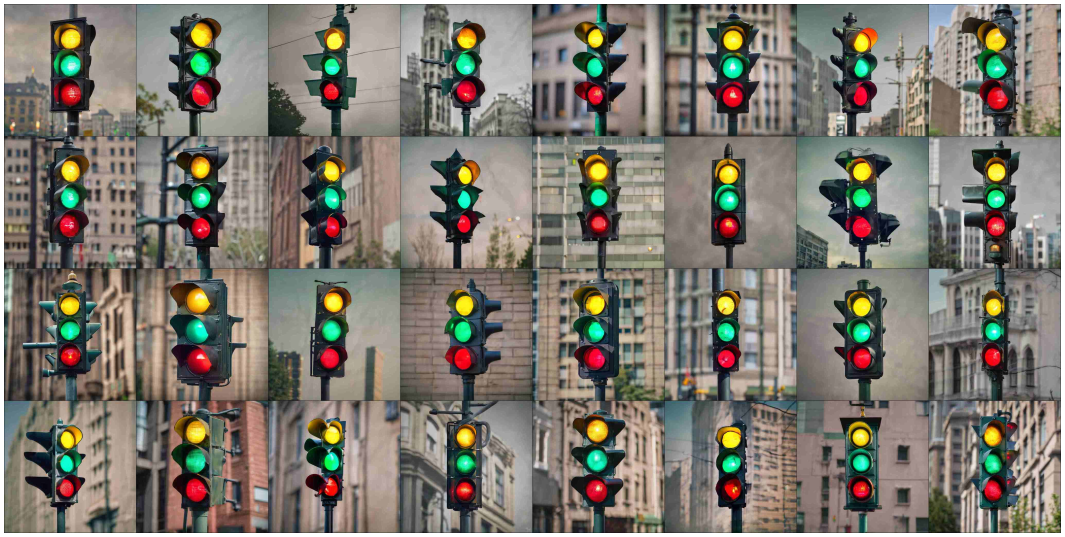

(b) Fast Direct

Figure 24: The 32 randomly generated image for the prompt ”traffic-light” guided by Fast Direct by utilizing 50 batch queries budget.

(a) Pre-trained

(b) Fast Direct

Figure 25: The 32 randomly generated image for the prompt ”apple” guided by Fast Direct by utilizing 50 batch queries budget.

(a) Pre-trained

(b) Fast Direct

Figure 26: The 32 randomly generated image for the prompt ”cyber-dog” guided by Fast Direct by utilizing 50 batch queries budget.

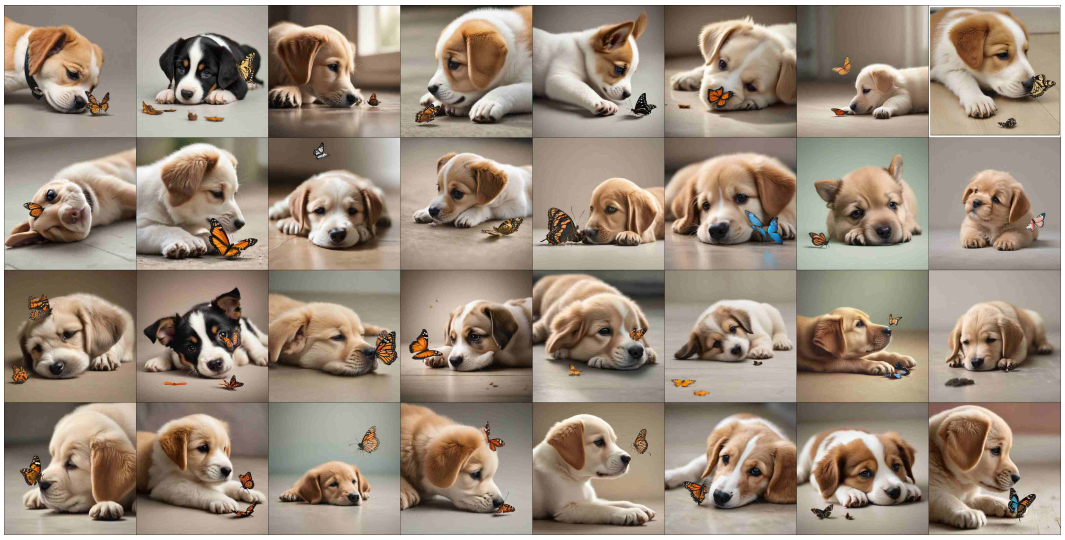

(a) Pre-trained

(b) Fast Direct

Figure 27: The 32 randomly generated image for the prompt ”puppy-nose” guided by Fast Direct by utilizing 50 batch queries budget.

(a) Pre-trained

(b) Fast Direct

Figure 28: The 32 randomly generated image for the prompt ”robot-plant” guided by Fast Direct by utilizing 50 batch queries budget.

(a) Pre-trained

(b) Fast Direct

Figure 29: The 32 randomly generated image for the prompt ”ocean” guided by Fast Direct by utilizing 50 batch queries budget.

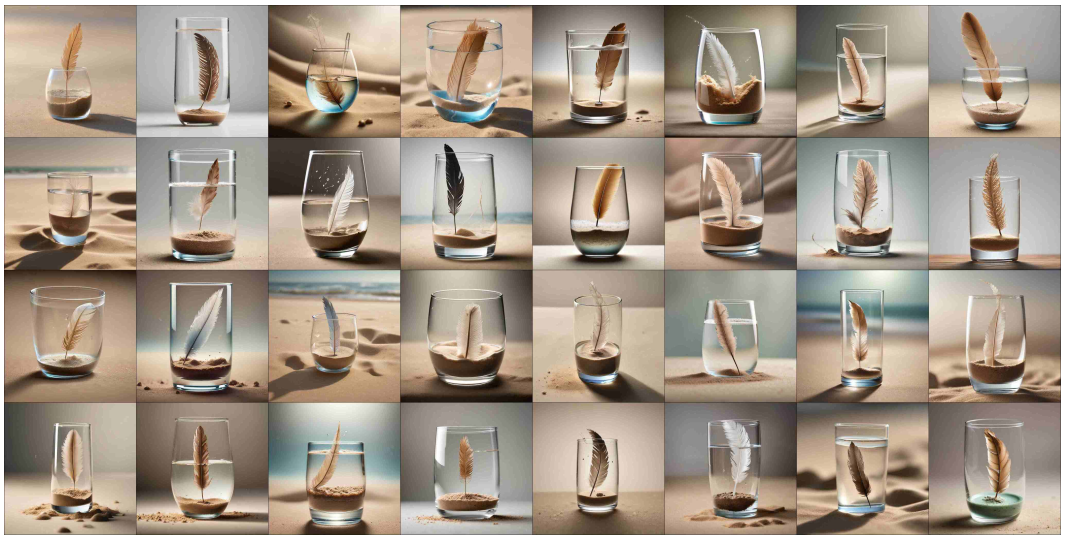

(a) Pre-trained

(b) Fast Direct

Figure 30: The 32 randomly generated image for the prompt ”sand-glass” guided by Fast Direct by utilizing 50 batch queries budget.

(a) Pre-trained

(b) Fast Direct

Figure 31: The 32 randomly generated image for the prompt ”penguin” guided by Fast Direct by utilizing 50 batch queries budget.

(a) Pre-trained

(b) Fast Direct

Figure 32: The 32 randomly generated image for the prompt ”basket” guided by Fast Direct by utilizing 50 batch queries budget.

(a) Pre-trained

(b) Fast Direct

Figure 33: The 32 randomly generated image for the prompt ”ice-cube” guided by Fast Direct by utilizing 50 batch queries budget.

(a) Pre-trained

(b) Fast Direct

Figure 34: The 32 randomly generated image for the prompt ”cat-butterfly” guided by Fast Direct by utilizing 50 batch queries budget.